LAWRENCE
LIVERMORE
NATIONAL
LABORATORY

Experiments and Modeling of Variably Permeable Carbonate Reservoir Samples in Contact with CO2-Acidified Brines

M. M. Smith, Y. Hao, H. E. Mason, S. A. Carroll

September 15, 2014

Disclaimer

This document was prepared as an account of work sponsored by an agency of the United States government. Neither the United States government nor Lawrence Livermore National Security, LLC, nor any of their employees makes any warranty, expressed or implied, or assumes any legal liability or responsibility for the accuracy, completeness, or usefulness of any information, apparatus, product, or process disclosed, or represents that its use would not infringe privately owned rights. Reference herein to any specific commercial product, process, or service by trade name, trademark, manufacturer, or otherwise does not necessarily constitute or imply its endorsement, recommendation, or favoring by the United States government or Lawrence Livermore National Security, LLC. The views and opinions of authors expressed herein do not necessarily state or reflect those of the United States government or Lawrence Livermore National Security, LLC, and shall not be used for advertising or product endorsement purposes.

GHGT-12

Experiments and modeling of variably permeable carbonate reservoir samples in contact with CO$_2$-acidified brines

Megan M. Smith*, Yue Hao, Harris E. Mason, and Susan A. Carroll

Atmospheric, Earth, and Energy Division, Lawrence Livermore National Laboratory, Livermore, CA, 94609 USA

Abstract

Reactive experiments were performed to expose sample cores from the Arbuckle carbonate reservoir to CO$_2$-acidified brine under reservoir temperature and pressure conditions. The samples consisted of dolomite with varying quantities of calcite and silica/chert. The timescales of monitored pressure decline across each sample (and concurrent increases in permeability) in response to CO$_2$ exposure, as well as the amount of and nature of dissolution features, varied widely among these three experiments. For all samples cores, the experimentally measured initial permeability was at least one order of magnitude or more lower than the values estimated from downhole methods. Nondestructive X-ray computed tomography (XRCT) imaging revealed dissolution features including "wormholes," removal of fracture-filling crystals, and widening of pre-existing pore spaces. In the injection zone sample, multiple fractures may have contributed to the high initial permeability of this core and restricted the distribution of CO$_2$-induced mineral dissolution. In contrast, the pre-existing porosity of the baffle zone sample was much lower and less connected, leading to a lower initial permeability and contributing to the development of a single dissolution channel. While calcite may make up only a small percentage of the overall sample composition, its location and the effects of its dissolution have an outsized effect on permeability responses to CO$_2$ exposure. The XRCT data presented here are informative for building the model domain for numerical simulations of these experiments but require calibration by higher resolution means to confidently evaluate different porosity-permeability relationships.

---

* Corresponding author. Tel.: +1-925-423-7970.
   E-mail address: megan@llnl.gov

1. Introduction

Several large-scale subsurface carbon utilization and sequestration projects have been implemented in response to rising levels of atmospheric carbon dioxide (CO_2). Desirable candidate sequestration scenarios include current and former CO_2-enhanced-oil-recovery fields, which can be transitioned into long-term CO_2 storage sites given the presence of sufficiently impermeable "seal" formations. As a result of the high reactivity of carbonate minerals such as calcite and dolomite under CO_2-acidified conditions, these carbonate reservoir formations can be expected to respond to CO_2 injection near the injection zone with generation of new pore space and potentially beneficial permeability enhancements as CO_2-charged fluids partially dissolve carbonate host minerals until reaching chemical equilibrium. However, this same type of reaction can also lead to the formation of less desirable fast fluid pathways in seal formations that contain carbonate minerals, and these preferential pathways could allow leakage of CO_2 into overlying geologic units.

A full understanding of the impact of chemical and mechanical stresses (e.g., fluid-mineral disequilibria, fluctuating reservoir conditions, etc.) resulting from CO_2 injection, and accurate predictions of how these stresses translate into meaningful changes in permeability throughout storage formations, is an active area of research [e.g., 1-6]. To address these questions, we present current results from several core-flood experiments, conducted at *in situ* storage temperature and pressure conditions, on well-characterized carbonate reservoir core samples from a potential carbon storage site (Wellington, Kansas, USA). The purpose of these experiments was to explore the effects of physical (pore connectivity, distribution) and chemical (calcite/dolomite/non-carbonate mineralogy) heterogeneity on the evolution of permeability within these core samples. To quantify these attributes, each sample was imaged via X-ray microtomography both prior to and after each brine-CO_2 core-flooding experiment. Geochemical fluid samples were collected throughout each experiment and interpreted to define each sample's approach to specific fluid-mineral saturation states.

Our experimental methodology was informed by a previous set of similar experiments, conducted on smaller low-permeability carbonate samples from an existing carbon storage site (the Weyburn-Midale CO_2-enhanced oil recovery and carbon storage site, Saskatchewan, Canada), [7,8]. In that work, we intentionally varied the pCO_2 of the flooding brines to examine effects on porosity and permeability evolution within spatially clustered samples selected for their similar mineralogy. In this study, our objective was instead to examine a range of larger-volume samples possessing a wider range of permeabilities and mineral contents, while holding the $CO_{2(aq)}$ content of the brine constant. The studies performed at the Wellington, Kansas field site by the Kansas Geological Survey (links and information accessible at [9]) included extensive characterization of the Arbuckle Group and other neighboring carbonate formations, which enabled us to select sample cores encompassing both reservoir and "baffle" zone formations and spanning over 3-4 orders of magnitude of expected permeability.

2. Materials and Methods

Sample cores of 38.1-mm diameter (1.5-inch) and variable lengths were obtained from the Kansas Geological Survey (Lawrence, Kansas, USA), and then polished at both ends to obtain flat surfaces. These samples were imaged both prior to and after reaction with CO_2-acidified brines, via X-ray computed tomography (XRCT). The experiments were carried out in a pressurized core-flooding reactor where temperature and pressure were held at roughly *in situ* values (60 °C and 24.8 MPa confining pressure). Fluid samples from each experiment were collected for geochemical analysis and differential pressures across the core samples were monitored during constant flow conditions.

2.1. Carbonate core samples

The samples in these experiments were provided from wells drilled into the Arbuckle group (a large Cambrian-Ordovician carbonate reservoir underlying much of Kansas) in the Wellington field of southern Kansas, as part of the South-central Kansas CO_2 Project [9,10]. The samples consist primarily of dolomite, with variable quantities of calcite (most commonly in the form of cement but also as isolated bands) and silica/chert. These particular core

samples were selected on the basis of their estimated bulk permeability (Table 1). The downhole value overpredicts each subcore's permeability. This difference may stem from the smaller volume of the subsample compared to that measured by the downhole tool, and it may also reflect uncertainty in the extraction of permeability data from downhole data collected in carbonate (as opposed to sandstone) reservoirs. Mason et al. (in this issue) more fully discusses improvements to prediction of carbonate permeability from similar samples using neutron magnetic resonance methods.

The uppermost sample, KS4737, was taken from a region identified as a "baffle" zone (a zone of slightly lower permeability). From examination of pre-reaction tomography data, this sample appears to consist of a porous dolomitic matrix in which pore spaces have been partially to fully filled with later-stage light gray-scale (calcite-rich) cement material (Figure 1a) and possibly replacement silica as well. According to well logs, sample KS4906 was taken near a boundary between an identified baffle zone and the typical injection zone target formation. From both core logs and visual inspection, this sample consists of intermittent regions of large dolomite rhombs (~2-4mm) within a predominantly fine-grained, massive dolomite matrix, with most visible pore space associated with the crystalline regions (Figure 1b). The deepest sample, KS4986, is taken from a thick interval of the Arbuckle target injection zone. Portions of this sample appear texturally similar to the partially re-cemented dolomite seen in KS4737, but a large volume of this core consists of a fractured, low-porosity darker gray-scale material (see Figure 1c). Some fractures are difficult to segment as their aperture (perpendicular to flow direction) is 1 pixel or less, but many fractures display maximum apertures of up to 10-15 pixels (425-630 microns). Where these fractures extend into the partially porous/re-cemented dolomite regions, they are completely sealed with lighter gray-scale material; within the fractured darker gray-scale material, euhedral calcite crystals are present but do not completely occlude the fractures.

Core log descriptions of all samples indicated that variable quantities of chert may be present, and siliceous material has been tentatively identified in some XRCT images based on shape and texture. In sample 4986 in particular, the fractured nature of the darker gray-scale material discussed above supports the possibility that it is microcrystalline silica. Distinguishing dolomite from a silica phase within the image datasets is problematic because at these XRCT scan conditions, both minerals may produce similar gray-scale values. Destructive sectioning of the reacted cores is underway to produce specimens for scanning electron microscopic determination of the abundance of chert/silica phases in selected regions.

Table 1. Carbonate core samples used in experiments.

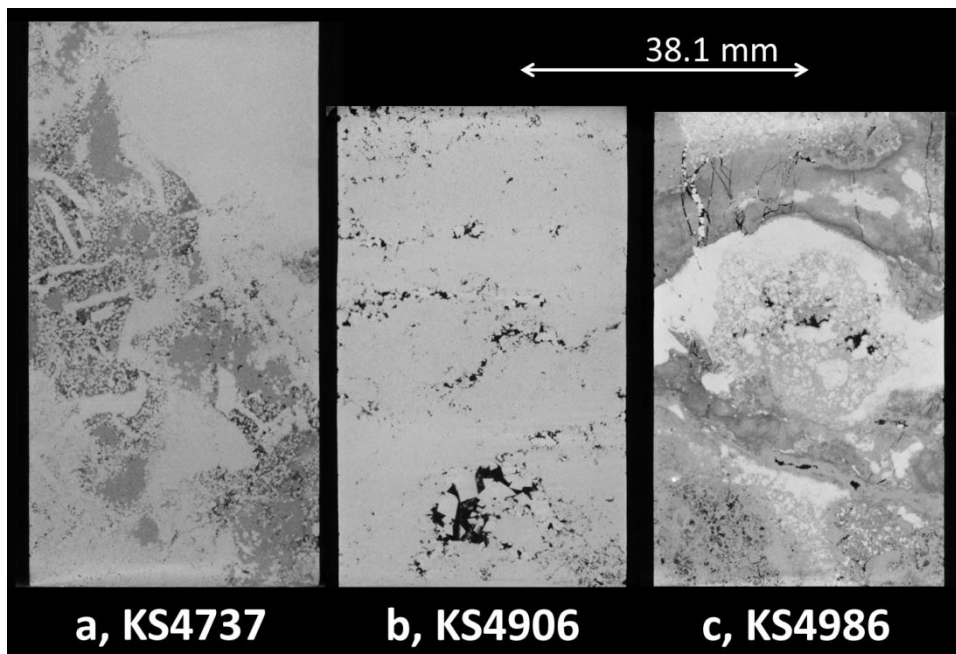| Sample identifier, formation type	Downhole interval bulk permeability, mD	Experimentally determined (initial) sample permeability, mD
KS4737, baffle zone	0.66	0.0012
KS4906, boundary	6.9	0.017
KS4986, injection zone	4.7	0.60

Fig. 1. Longitudinal cross-sections from XRCT imaging of samples (a) KS4737; (b) KS4906; and (c) KS4986. Gray-scale in these XRCT images is proportional to phase density; therefore, voidspace is represented by a low gray-scale (i.e., black).

2.2. Experimental methods

The three experiments discussed here follow the same experimental methodology and were carried out in the same experimental set-up discussed in [7]. Modifications to the system included new endcaps to accommodate the larger Arbuckle cores, and additional valves to allow switching among CO_2-free brine, CO_2-free/tracer-spiked brine, and two pressurized CO_2-brine mixer vessels. For comparison between these experiments and those conducted previously on calcite-rich cores from the Weyburn-Midale, Canada, enhanced oil recovery and storage site, the same brine composition was utilized: ~1.1 molal NaCl solution containing lower quantities of $NaHCO_3$, $CaCl_2$, and $MgCl_2$ to ensure equilibrium or slight supersaturation with respect to calcite and dolomite in the absence of dissolved CO_2. During CO_2/brine flow periods, brine pCO_2 was maintained at or near 3 MPa, ensuring undersaturation of the input solution by at least two orders of magnitude with respect to both calcite and dolomite.

After pre-reaction XRCT imaging, each experiment followed the same protocol: brine saturation; pre-reaction tracer test; pre-CO_2 flow and sampling to collect baseline geochemical and pressure/permeability data; CO_2/brine flow with differential pressure monitoring and geochemical sample collection; post-reaction tracer test and final permeability measurements; N_2 gas flush to remove brine. The samples were reacted at 60 °C, under constant 24.8 MPa confining pressure and 12.4 MPa outlet pressure. The experiments were conducted under constant flow rate conditions (0.34 mL min^{-1}, unless noted otherwise) so that changes in differential pressure across the core could be correlated to changes in bulk sample permeability. The flow rate was chosen to maintain the same Darcy flux through these larger samples as had been utilized in the previous Weyburn core experiments [7]. One experiment using sample KS4737 had to be conducted at a slower flow rate (0.034 mL min^{-1}) due to the sample's lower permeability. A heat-shrinkable fluorelastomer jacket covering the sample and both endcaps effectively isolated the brine flowing within the core from the pressurizing fluid inside the reactor vessel.

Outlet fluid samples were collected and filtered to monitor major and trace elements, and total inorganic carbon was sampled via alkaline trapping of outlet fluids and exsolving $CO_{2(g)}$. Prior to the introduction of CO_2-enriched brine, solution pH was monitored during sampling events. During CO_2/brine flow periods, solution pH (at 60 °C)

and saturation indices (indicating the degree of saturation of the fluid with respect to minerals of interest) were modeled using the EQ3/6 geochemical speciation code and the *data.shv* thermodynamic database [11, 12].

2.3. X-ray computed tomography imaging and data methods

Each sample was imaged before and after reaction via XRCT using an Xradia microCT scanner and cone-beam data acquisition at the University of Austin Computed Tomography Laboratory (Austin, Texas, USA). Scans were conducted at 90 keV with a SiO_2 filter, using the same objective and detector/source distances, to consistently produce a voxel resolution of 42.55 microns. The length of the cores necessitated data collection in separate parts which were automatically stitched together using Xradia software.

Both 16-bit and 8-bit image stacks were collected but image analysis was performed on 8-bit stacks only for efficiency. The two XRCT datasets generated from each sample were registered and aligned via (*x,y*) translation and rotation using the Align3_TP plugin and Fiji/ImageJ software [13, 14]. After analysis of gray-scale images and histograms, the post-reaction dataset was segmented into binary black/white images (representing porous space versus solid mineral phases) which were then applied as a mask to the pre-reaction images. The masking method described here thus produces a final image stack representing all identifiable pore space present after reaction, including all void volumes that existed prior to reaction.

Segmentation of each sample's post-reaction image stacks was performed at two specific gray-scale values. Use of the lower value systematically omitted small pores (1-3 pixels) from the segmentation as a result of partial-volume effects, while use of the higher threshold value increased the segmented volume of larger regions of reactive dissolution by including partially porous reactive rinds in the final segmented pore volume. In this discussion we present results obtained from segmentation using the upper gray-scale boundary for pore space (see section 3.2) to represent more of the smaller-scale pore features still visible at the 42.55-micron image resolution. Overestimation of void volume will most likely occur in regions of focused dissolution in porous regions (i.e., channel features or "wormholes" with skeletonized reaction rims), which are not the primary type of dissolution feature formed in two of the three experiments.

Higher-resolution imaging (obtained via destructive subsampling of the reacted core samples) is necessary to better characterize both the micro-pore distribution and specific mineral composition of regions or phases with specific gray-scales; these analyses will be conducted in order to more accurately compare tomography results with estimates of mineral dissolution obtained from solution geochemistry. Pending this higher-resolution analysis, we will refer to solid phases primarily by their gray-scale, with likely corresponding mineral phase in parentheses. No regions of newly produced solid phases (i.e., precipitated minerals) were noted via comparison between the two datasets; this finding is consistent with the interpretation of the geochemical data (see section 3.3, below).

3. Results and discussion

3.1. Permeability evolution with time

The timescale of the pressure decline across each sample (and concurrent increase in permeability) in response to CO_2 exposure varies widely among these three experiments (Figure 2). As CO_2-acidified brine was introduced into each core sample, the differential pressure across each sample decreased to levels below the accuracy of the two transducers over time periods from 10 hours to 50 days. Note that the KS4737 experiment (baffle zone sample) had to be conducted at a slower flow rate (0.034 mL min^{-1}) to bring its initial differential pressure below our experimental reactor's limits. These pressure data are extremely valuable for constraining our numerical modeling efforts.
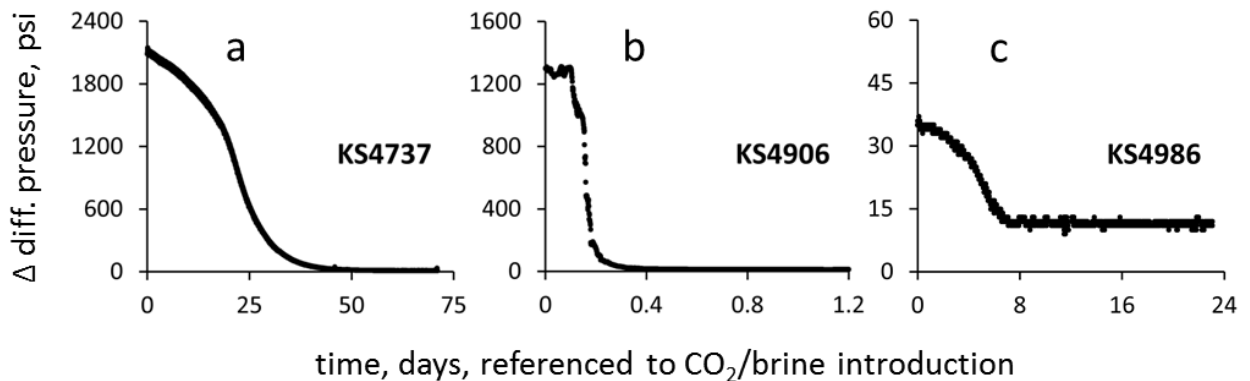
Fig. 2. Differential pressure from core inlet to outlet ("Δ diff pressure") versus time from experiments with samples KS4737 (a); KS4906 (b); and KS4986 (c). Note that samples KS4906 and KS4986 were reacted at a constant flow rate of 0.34 mL min^{-1}, while sample KS4737 required a slower flow rate of 0.034 mL min^{-1}.

3.2. XRCT results

XRCT datasets were collected from samples both prior to and after each reactive flow experiment. Figures 3-4 and 7 show several rotated views of 3-dimensional segmented pore space volumes from each sample, post-reaction. Note that pre-existing pore spaces (void volumes which were identified in both pre- and post-reaction imaging as experiencing no change) are shown in white, while regions of newly produced pore space (previously identified as solid mineral phases in pre-reaction imaging) are shown in various shades of darker gray-scale.

Sample KS4906 (taken from an intermediate boundary between "baffle" and injection zones) possessed abundant initial porosity but no fully connected pore network at the scale of the XRCT imaging conducted prior to reaction with CO_2-acidified brine (Figure 3a). After the short (< 3-day-long) experiment, only very small quantities of solid phase removal could be detected in the XRCT image data, and registration of the two datasets introduced error on the same scale. Complete registration of the image "stacks" was also complicated by apparent shifting of some rhombic crystals (i.e., "landmarks" did not remain consistent). Therefore, both pre- and post-reaction XRCT images are shown in Figure 3, with connected pore clusters highlighted in different colors. It is likely that dissolution of small key regions such as those indicated by arrows in Figure 3 was responsible for this sample's extremely rapid decline in differential pressure/increase in permeability (occurring in less than 10 hours). Reexamination of the gray-scales of the dissolved regions shows that the dissolved material possessed slightly lighter gray-scale values compared to neighboring pixels but the difference was small compared to overall matrix gray-scale variability.

In the injection zone sample (KS4986), however, XRCT imaging reveals that multiple fractures, concentrated in the downstream half of the core and oriented roughly along the direction of flow, may have contributed to the relatively high initial permeability of this core (Figure 4a, upper half of image/downstream portion of sample). From pre- and post-reaction image comparison, it can be seen that reaction with CO_2-acidified brine effectively dissolved light gray-scale (calcite) crystals present within some of these fractures (Figure 5). Previously sealed fractures extending into more porous regions near the inlet were also excavated by the end of the experiment (Figure 6). Instances of localized dissolution of bright gray-scale material (calcite; see large red rounded regions in right side of Figure 4c) were observed to occur only in close proximity to an existing fracture. No dissolution of the surrounding darker gray-scale material comprising the walls of the fractures was noted, however, lending support to its identification as silica rather than a dolomite matrix.

In contrast, the pre-existing porosity of the baffle zone sample KS4737 (shown in green color, Figure 7) is much lower than the previous two cores, and consists primarily of dispersed and unconnected small pore spaces; the resulting low permeability in this sample necessitated the use of a slower flow rate for the experiment. CO_2/brine flow in this sample resulted in the formation of one large through-going dissolution channel or "wormhole" (Figure 7, red color). Based on comparison of pre- and post-reaction imaging, this dissolution channel originated within

lighter gray-scale (again, likely calcite) regions, but proceeded to widen during the course of the experiment through dissolution of surrounding darker gray-scale material. A skeletonized "rind" of darker gray-scale material (dolomite) is also evident around much of the developed channel. Comparable dissolution features, although lacking the partially dissolved rinds, were noted in the similarly less-permeability Weyburn "V-6" formation samples reacted at various pCO_2 levels [7].
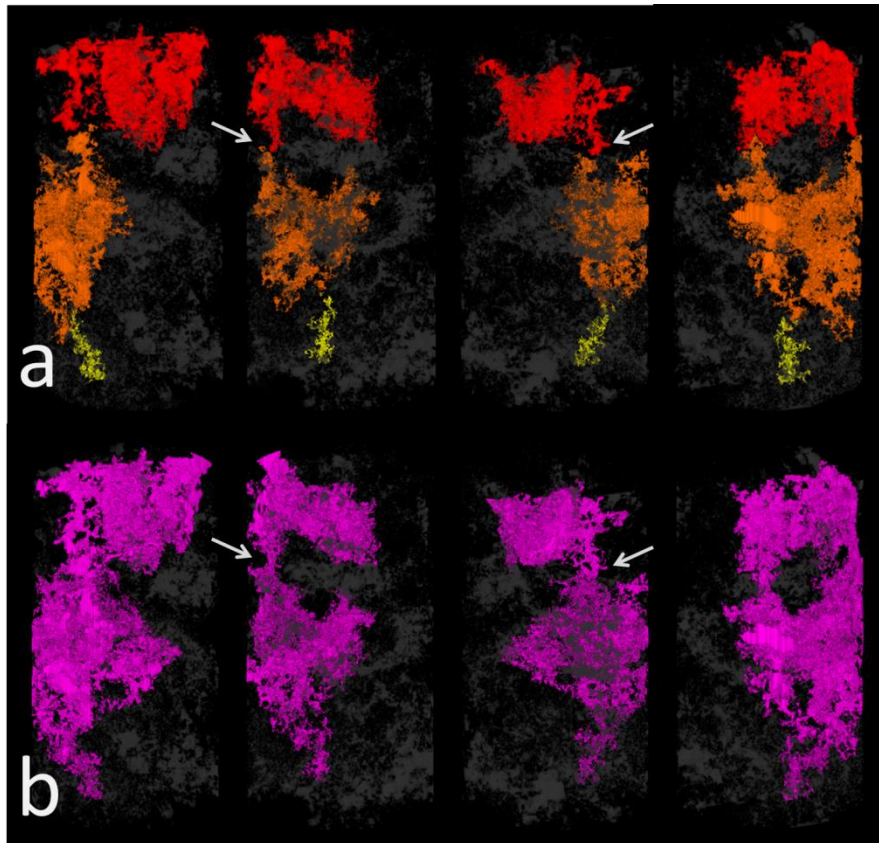

Fig. 3. 3-D representation of total porosity of boundary sample KS4906, four rotated views: 0, 90, 180, and 270°, from pre-reaction XRCT imaging (a) and post-reaction imaging (b). In this view brine flow direction was upward. All identified pore space was originally given a dark gray color, with specific connected pore networks identified by color. Note that in the pre-reaction images, several large connected pore clusters exist (red, orange, yellow colors) but none provide a fully connected pathway from sample inlet to outlet. In post-reaction imaging, small regions of dissolution (see arrows) allowed connection between the previously identified pore clusters.
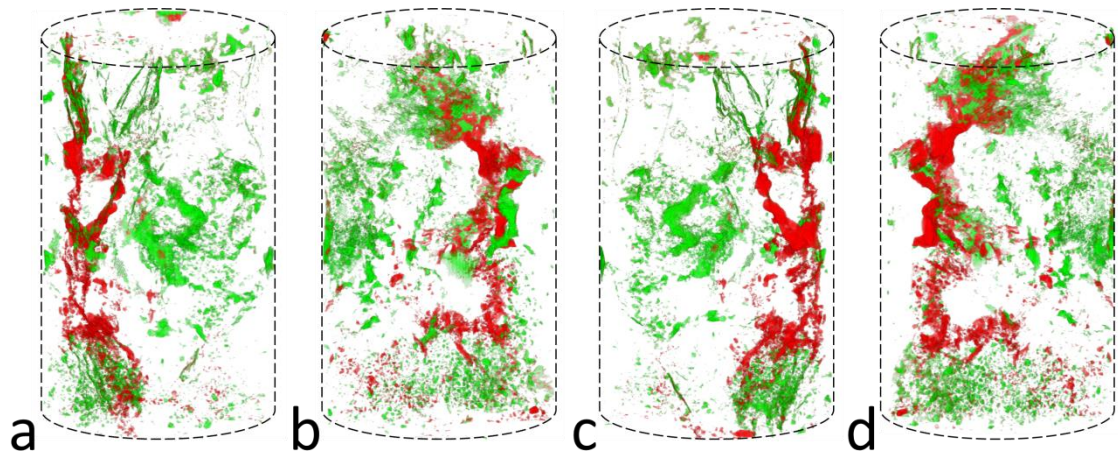
Fig. 4. Injection zone sample KS4986, four rotated views: 0° (a); 90° (b); 180° (c); and 270° (d) of the 3-D representation of total pore space present after CO_2/brine reaction. In this view brine flow direction was upward. Note that pre-existing pore space is shown in green, while pore space generated through reaction and dissolution of mineral phases is shown in red. The 0° view was selected to orient pre-existing (green color) fractures in the downstream (upper) half of the image.
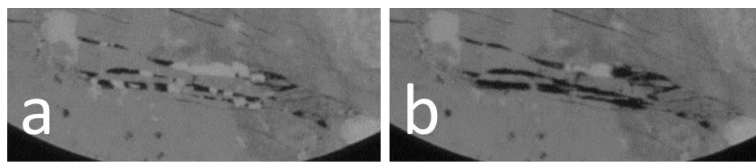

Fig. 5. Portions of cross-sectional images taken perpendicular to flow direction, 53 mm downstream of sample inlet, from sample KS4986 prior to (a) and after (b) CO_2/brine exposure. Light gray-scale crystals located within pre-existing fractures have been removed in post-experimental imaging. For scale, each image is approximately 18.5 mm in width.
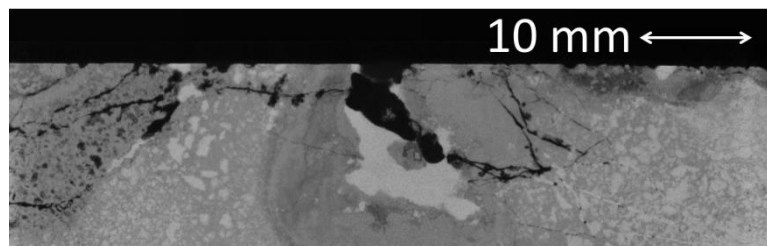

Fig. 6. Longitudinal cross-section from sample KS4986, post-reaction XRCT imaging (shown from a different radial angle than that in Figure 1c). Entire core length is shown in this view; brine flow proceeded from left to right. The fractures are present along the majority of the sample length, and are more clearly evident in post-reaction images as a result of dissolution and removal of solid material. Note that many fractures extend beyond the low-porosity dark gray-scale material (center) and into the variably cemented porous regions present at inlet and outlet.
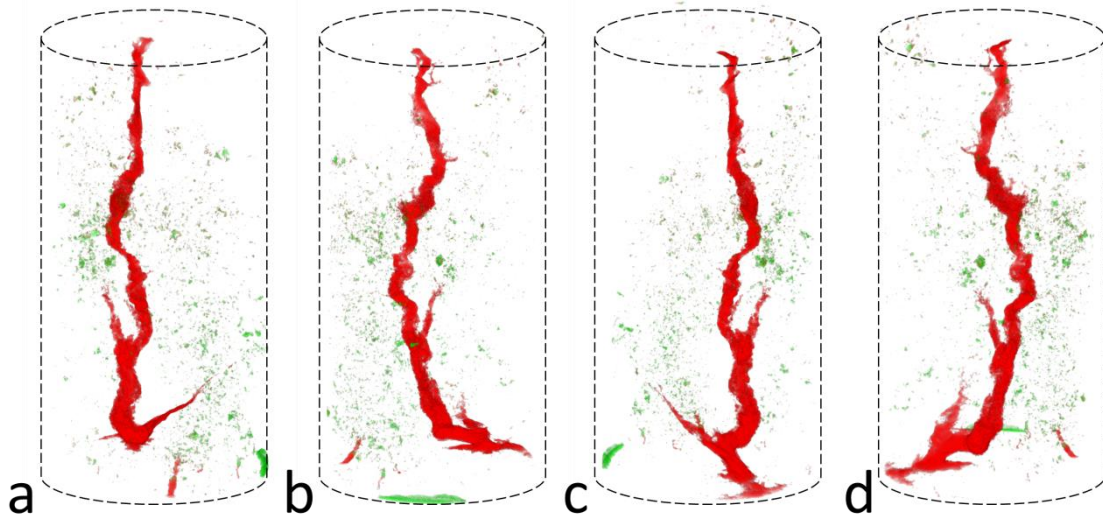
Fig. 7. Baffle zone sample KS4737, four rotated views: 0° (a); 90° (b); 180° (c); and 270° (d) of the 3-D representation of total pore space present after CO_2/brine reaction; brine flow direction is upward. Note that pre-existing pore space is shown in green, while pore space generated through reaction and dissolution of mineral phases is shown in red.

3.3. Solution geochemistry of reacted samples

We adopt here the same protocol for interpretation of geochemical data as described in [7]. Chloride concentrations were monitored to ensure correct charge balancing before correction of solution pH to 60 °C values via EQ3/6 geochemical speciation models. Dissolved silica was analyzed via ICP-MS for one sample with high uncertainty due to interfering matrix effects; thus $SiO_{2(aq)}$ concentrations were not included in our geochemical solution models. CO_2-free brine solutions were in equilibrium with disordered dolomite and were slightly supersaturated with respect to both calcite and ordered dolomite, with a solution pH of approximately 6.8-7.1 at 60 °C. After equilibration with 3 MPa pCO_2 the influent solution pH dropped to 3.8-4.2 at 60 °C, and the brine solution was undersaturated with respect to all carbonate minerals. Modeled saturation indices (*SI*, a measure of the fluid's equilibrium or disequilibrium with respect to minerals of interest) are shown for each experiment in Figures 7a-c. We show *SI* values for both an ordered and a disordered dolomite in these figures due to current uncertainty over which thermodynamic value is more appropriate for these samples. Note that the trends in model fluid-carbonate *SI* values mirror modeled solution pH values (which in turn are controlled primarily by measured total inorganic carbon levels). At late times, solution pH at the outlet of sample KS4906 approached 4.9-5.0. Sample KS4737 produced similar quasi-steady-state solution pH levels of ~4.8. Outlet pH levels for the KS4986 experiment were slightly lower (4.5), and were shown to decrease further still to 4.3 with the introduction of brine with higher pCO_2 level (3.7 MPa, at times *t* = 5.7 and 17 days, indicated by vertical arrows in Figure 7b). Effluent from samples 4986 and 4737 (injection and baffle zone samples) remained undersaturated with respect to calcite at all times in the presence of $CO_{2(aq)}$, while fluids from experiment KS4906 (boundary sample) eventually achieved calcite equilibrium after the sharp permeability increase due to connection via dissolution of a critical mineral volume. We note however in XRCT images that sample KS4906 contained only very small quantities of light gray-scale material identified as calcite or calcite-rich material; therefore our initial gray-scale/mineralogy calibration may be incorrect or may not fully account for intermixed fine-grained material or carbonate minerals of intermediate/impure composition.

Dissolved calcium and magnesium concentrations over time can provide independent estimates of the volumes of solid carbonate phases dissolved during $CO_{2(aq)}$ exposure (see Figures 7d-f). These interpretations of dissolved mineral quantities should be regarded as preliminary, because we assume our samples consist of perfectly magnesium-free calcite and dolomite with a perfect 1:1 calcium/magnesium ratio (see [7] for details of the

calculation), and because we neglect possible silica-phase dissolution. We concede that the first assumption may be inappropriate for a reservoir such as the Arbuckle which has experienced several episodes of secondary dolomitization events [10]; nevertheless, these calculations provide a starting point for interpretation and comparison of changes in porosity observed in XRCT data. According to this analysis, calcite accounted for a larger proportion of total mineral dissolution in the boundary zone sample, KS4906, than in the other two samples. Calcite and a "perfect" dolomite contributed roughly equally to new pore space generation via dissolution within the injection zone sample (KS4986), while dolomite contributed nearly twice as much as calcite in the buffer zone sample (KS4737). In some instances these geochemically derived estimates are plausible; for example, a rough estimate of several cross-sectional images of the wormhole feature in KS4737, comparing central areas of light gray-scale/calcite to annular regions of darker gray-scale/dolomite, is in approximate agreement with the 2:1 ratio. However, the XRCT data from sample 4906 do not support predominant dissolution of calcite relative to dolomite in our current gray-scale calibration. We are currently preparing sectioned samples for scanning electron microscopy and microprobe analysis of mineral composition in order to resolve these discrepancies.
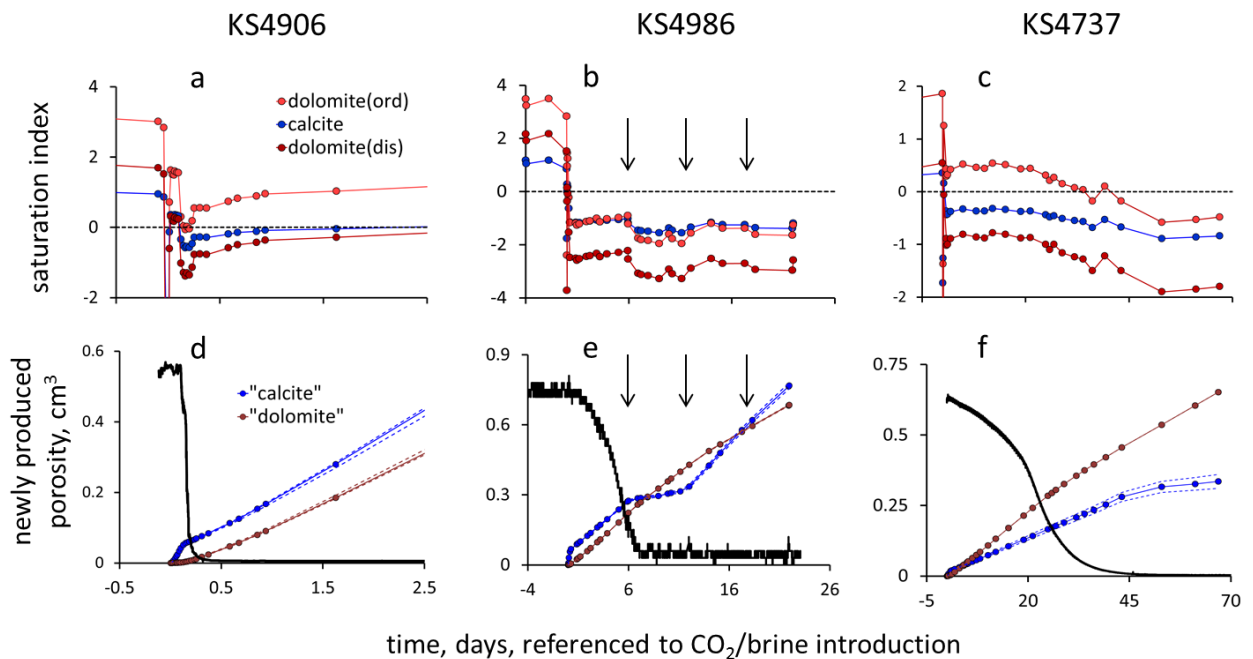

Fig. 7. Modeled fluid saturation indices (*SI*) with respect to calcite (blue) and dolomite (light red, ordered; dark red, disordered) versus time, for experiments KS4906 (a); KS4986 (b); and KS4737 (c). Dashed horizontal lines are provided at *SI* = 0 for purposes of comparison. Below each SI plot are corresponding estimates of newpore volumes generated through dissolution (cm^3) of specific carbonate minerals over time. Pressure decline curves are shown in heavy black for reference only. Arrows in figures 7b, 7e indicate experimental change-overs between separate CO_2/brine mixer vessels with slightly different pCO_2 levels (3 versus 3.7 MPa).

4. Current findings and ongoing work

Currently, three reactive flow experiments have been conducted on 38-mm diameter carbonate core samples from the Wellington 1-32 well, Kansas, USA, with five more experiments planned. Although some of these samples (particularly the injection zone sample, KS4986) were selected specifically for their high permeability according to downhole measurements, we find that in each case the experimentally measured permeability in the core subsample is lower than that estimated from the corresponding well interval. The downhole tool samples a larger representative rock volume and may be sensing contributions of larger vugs, fractures, or other features which may not be adequately represented in these subsamples.

While it is not surprising that calcite dissolution plays a key role in increasing pore space connectivity and bulk permeability in these samples (shown in post-reaction XRCT imaging), it is instructive to note that much of the calcite in these samples is present primarily in the form of more recent pore-filling cements or crystal formation postdating fracture formation. While calcite may make up only a small percentage of the overall sample composition, its location and the effects of its dissolution have an outsized effect on permeability responses to CO_2 exposure. We note also that within darker gray-scale areas identified as dolomite, more finely crystalline material appears to dissolve more readily than larger euhedral crystals, and that this material tends to dissolve only when in proximity to more reactive light gray-scale material (calcite). Mineral identification analyses will be performed on sacrificed core sections to quantitatively determine mineral distributions and to test support for many of our observations from the XRCT images.

The XRCT data presented here are informative for building the model domain for simulations of these experiments to test different fits to porosity-permeability relationships, but require calibration by higher resolution means in order to add confidence to the simulation outcomes. The geochemical data in combination with XRCT observations imply that small volumes of dissolved material as a result of the introduction of chemically reactive CO_2-acidified brine can lead to large increases in connected pore or storage space, benefitting the longevity of injection zones. Better gray-scale differentiation between silica and dolomite phases and the determination of impurities in carbonate minerals will inform our modeling efforts and add confidence to our geochemical interpretations. The form of the dependency of resulting permeability on the pace and extent of CO_2-carbonate mineral reactions in particular must be evaluated in a robust simulation framework. Currently these experiments are being simulated using the NUFT reactive transport code following the methodology of [8] and including new techniques for incorporating fracture flow and matrix diffusion.

Acknowledgements

References

[1] Golfier F, Zarcone C, Bazin B, Lenormand R, Lasseux D, Quintard M. On the ability of a Darcy-scale model to capture wormhole formation during the dissolution of a porous medium. J Fluid Mech 2002;457:213-254.

[2] Luquot L, Gouze P. Experimental determination of porosity and permeability changes induced by injection of CO_2 into carbonate rocks. Chem Geol 2009;265:148–59.

[3] McDuff D, Jackson S, Shuchart C, Postl D. Understanding wormholes in carbonates: unprecedented experimental scale and 3D visualization. J Petrol Technol 2010;62:78-81.

[4] Ellis P, Peters C, Fitts J, Bromhal G, McIntyre D, Warzinski R, Rosenbaum E. Deteriorioation of a fractured caprock exposed to CO_2-acidified brine flow. Greenhouse Gases Sci Technol 2011;1:248-260.

[5] Mason HE, Du Frane WL, Walsh SDC, Dai Z, Charnvanichborikarn S, Carroll SA. Chemical and mechanical properties of wellbore cement altered by CO_2-rich brine using a multi-analytical approach. Env Sci & Technol 2013;47:1745-1752.

[6] Walsh SDC, Mason HE, Du Frane WL, Carroll SA. Experimental calibration of a numerical model describing the alteration of cement/caprock interfaces by carbonated brine. Int J Greenhouse Gas Control 2014;22:176-188.

[7] Smith MM, Sholokhova Y, Hao Y, Carroll SA. CO_2-induced dissolution of low permeability carbonates. Part I: Characterization and experiments. Adv Water Res 2013;62 part C:370-387 .

[8] Hao Y, Smith M, Sholokhoa Y, Carroll SA. CO_2-induced dissolution of low permeability carbonates. Part II: Numerical modeling of experiments. Adv Water Res 2013;62 part C; 388-408.

[9] http://www.kgs.ku.edu/PRS/Ozark/well_1_32.html; last accessed 10 September 2014.

[10] Franseen EK, Byrnes AP, Cansler JR, Steinhauff DM, Carr TR. The Geology of Kansas – Arbuckle Group. In: Current Research in Earth Sciences: Kansas Geological Survey, Bulletin 250, part2.

[11] Wolery TW. EQ3/6. A software package for geochemical modeling of aqueous systems: Package overview and installation guide (version 7.0). UCRL-MA-110662-PT-1, Lawrence Livermore National Laboratory, Livermore, CA, USA, 1992.

[12] Johnson JW, Oelkers EH, Helgeson HC. SUPCRT92: A software package for calculating the standard molal thermodynamic properties of minerals, gases, aqueous species, and reaction from 1 to 5000 bar and 0 to 1000 °C. Comput Geosci 1992;98:131-139.

[13] http://www.med.harvard.edu/jpnm/ij/plugins/Align3TP.html; last accessed 28 August 2014.

[14] Rasband WS. ImageJ. U.